Evaluation of an LED Printer and Printhead using Print Quality Analysis

Luo Cheng, David Forrest and Ming-Kai Tse
Quality Engineering Associates (QEA), Inc.
Burlington, Massachusetts, USA

Abstract

To satisfy the demand for higher quality, manufacturers of LED print heads for electrophotography need effective measurement tools, both for quality and process control in production and for research and development. For LED printers, mid-tone gray-level uniformity is one of the key quality attributes. Because the print quality is very sensitive to print head performance, using carefully designed test targets with a commercially available image quality analysis system, LED print head quality can be quantified and characterized. This paper describes a measurement and diagnostic method of LED print heads and non-uniformity characterization using banding and line analysis tools. An advanced signal processing technique, discrete wavelet transform, was applied to decompose the signal and extract key information for LED print head quality. The correlation between vertical banding and LED print head defects will be discussed via a case study.

Introduction

As an alternative to laser printers, LED printers use an LED bar as a light source to replace scanning laser devices. Figure 1 illustrates the structure of a section of an LED bar from a print head. Figure 1 (a) was captured with external illumination turned on to reveal the LED packaging and surrounding components (lens removed) while Figure 1 (b) was captured with external illumination off. The quality of the LED bar has a direct impact on the print quality. Variations in individual LED element intensity and their spacing on the bar will cause problems of non-uniformity such as vertical banding.

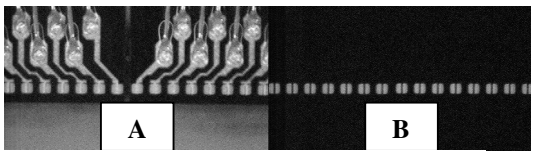

Figure 1. Structure of LED bar.

The focus of this paper is an indirect measurement of the print head quality using printed samples. Two print targets were used: a line pattern target and a 50% gray pattern. Some measurements were also made directly on the LED print head using a camera-based image analysis system.

Experimental

The print quality analysis system used in this study is the QEA IAS-1000 automated image analysis system, the first commercially available system to incorporate the ISO-13660 standard. The system typically includes a CCD camera with high-resolution optics, light source, frame grabber and a vacuum-equipped X-Y motion stage for positioning and holding samples. IAS-1000 has a set of built-in functions for print quality analysis including dot, line and large area quality metrics. In this investigation, the built-in banding tool and line tool were used to characterize the uniformity of an LED printer and print head.

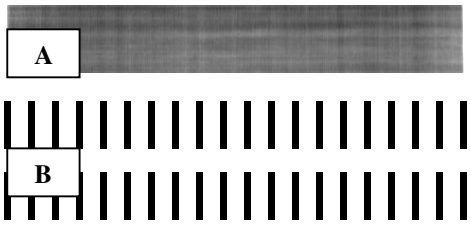

Figure 2. Test Target, (a) 50% Gray Pattern; (b) Line Pattern

In developing diagnostic methodologies for automated print quality analysis, appropriate design of the test target is critical. To characterize non-uniformity across the page, a 50% gray page created in Adobe Photoshop was printed to reveal the non-uniformity in the print density in an Okidata Okipage 8z LED printer (300 dpi, 84μm addressability) as shown in Figure 2 (a). The print shows prominent vertical banding, horizontal banding, and large area non-uniformity. The vertical banding may be caused by defects in the LED array. Based on our previous experience in inkjet print head inspection,[1] we used line analysis techniques on a specially designed test target to evaluate the LED print head. A pattern of one pixel wide lines, each printed from a single LED spaced so that each line is clearly resolved, satisfies

the target design for LED quality inspection. A very small portion of this target is shown in Figure 2 (b). In this study, a 300 dpi pattern of 1 on 9 off lines was printed. The lines are 84 µm wide and are spaced 840 µm from center to center. This pattern was repeated 10 times with successive 84 µm offsets, so that at the top of the page pixels 1, 11, 21, …, 2391 were active, and below this pattern pixels 2, 12, 22, …, 2392 were active, and so on until the final (tenth) pattern where pixels 10, 20, 30, …, 2400 were active. This pattern facilitates measurements related to individual LED pixels, specifically line position and width.

To perform the measurements, an automated test sequence was created which analyzed both the full-page gray pattern test target and line pattern target. The IAS-1000 magnification was set to 5 µm/pixel. The gray sample was measured using the banding analysis tool, which develops a reflectance profile across the entire page width. The line pattern target was measured and the data were compiled using the line measurement tools in the IAS-1000.

To verify the effectiveness of these indirect measurements, we also measured the LED pixels directly using IAS-1000. For these measurements, the LED bar was removed from the printer. To obtain high contrast images, the standard light source on IAS-1000 was turned off and the LED array was turned on. Standard line tools in the IAS-1000 software were used to measure the position and strength of LED pixels directly.

Results and Discussion

Banding and Gray-Level Non-uniformity Characterization

The IAS-1000 banding tool automatically collected the reflectance profile and plotted the data using Microsoft Excel as shown in Figure 3. The banding tool uses FFTs to determine the component frequencies of the reflectance profiles as shown in Figure 4. The sample shows prominent low frequency gray-level non-uniformity across the page as well as high frequency bands. Different metrics can be used to describe the severity of this non-uniformity / banding and details can be found in the previous research.[2] In this study, a relatively new technology, wavelet transform, was applied to analyze the reflectance profile at different resolutions.

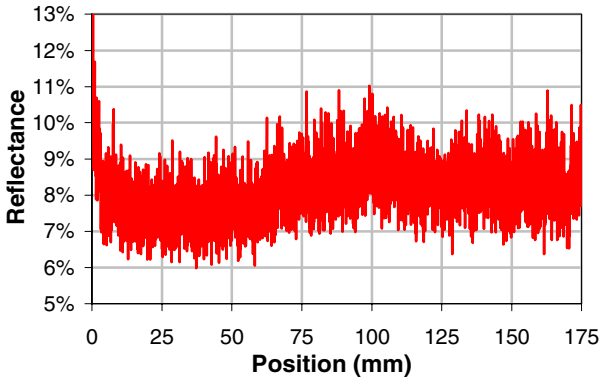

Figure 3. Reflectance profile.

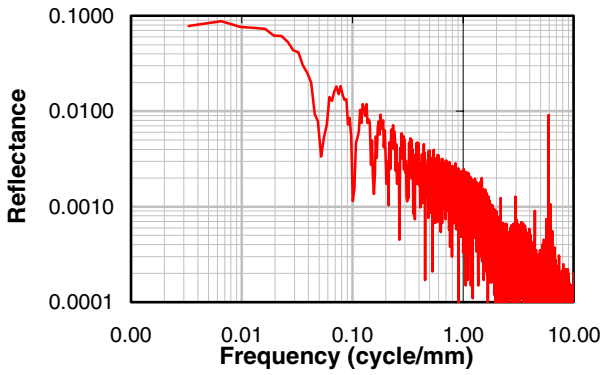

Figure 4. Frequency spectrum of reflectance profile.

The discrete wavelet transform (DWT) is a fast, linear, invertible and orthogonal operation,[3] just like the discrete Fourier transform. The basic idea lying under the discrete wavelet transform is to define a time-scale representation of a signal by decomposing it onto a set of basic wavelet functions. Wavelets are obtained from a single prototype wavelet, called the mother wavelet, by scaling and shifting. One of the advantages of DWT is that it is suitable for the analysis of non-stationary signals since it allows simultaneous localization in time and in scale. Application of the DWT results in a multilevel decomposition of the input signal into high and low frequency components in different resolutions according to the number of levels employed, as shown in Figure 5 (a) and (b). Figure 5 (a) illustrates a single stage filtering process where H is a high-pass filter and G is a low-pass filter. The original signal, S, passes through two complementary filters and emerges as two signals A and D which are known as "approximations" and "details," respectively. The approximations are the low-frequency components of the signal. The details are the high-frequency components. The decomposition process can be iterated, with successive approximations being decomposed in turn, so that one signal is broken down into many lower-resolution components, represented on a wavelet decomposition tree as shown in Figure 5 (b).

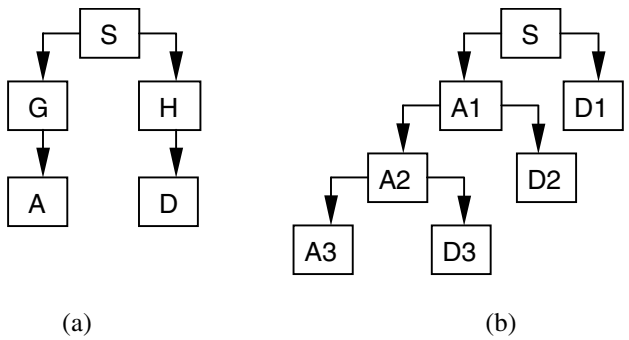

Figure 5. (a) Single stage decomposition. (b) Multiple stage decomposition.

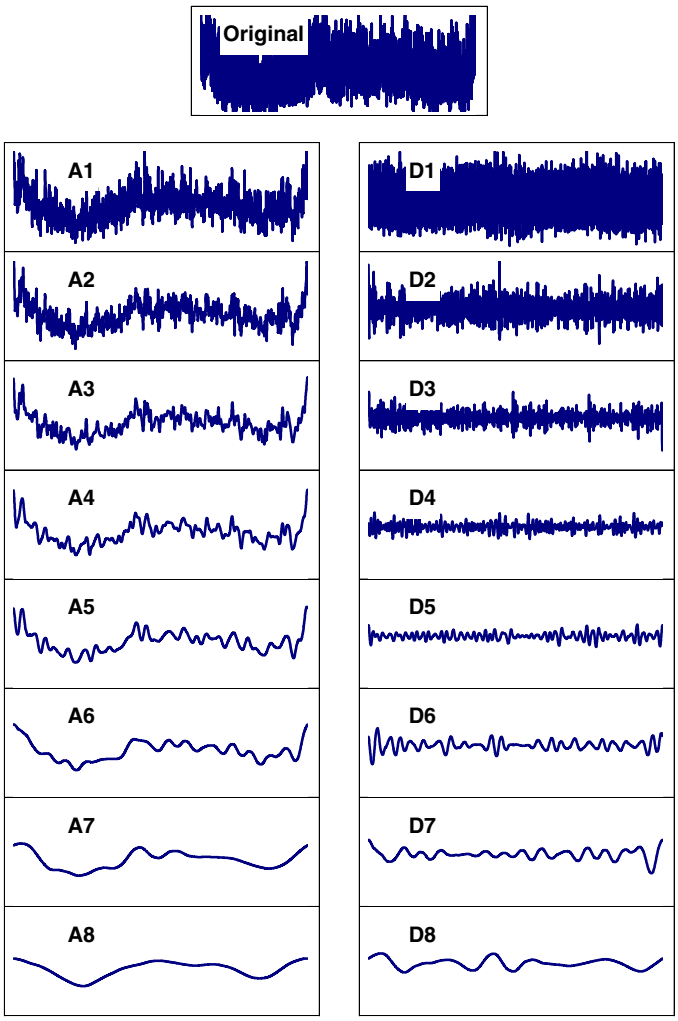

Figure 6. Wavelet decomposition of reflectance profile.

An example of wavelet decomposition is illustrated in Figure 6. The reflectance profile from the 50% gray pattern was decomposed in eight levels corresponding to eight resolutions from high to low. The wavelet used in this example is the Daubechies 12. Each successive decomposition has a cut-off frequency equal to one-half of the previous iteration. Decomposed signal A1 includes frequency components at approximately 11 cycles/mm and lower; decomposed signal A2 includes components at approximately 5.6 cycles/mm and lower. Both of these signals include noisy high frequency reflectance variations which are not normally objectionable to human observers. Decomposed signals A3 (cutoff frequency approximately 2.7 cycles/mm) to A5 (cutoff frequency approximately 0.7 cycles/mm) highlight the reflectance variations which are perceived as "banding" defects by human observers at a normal viewing distance. Decomposed signals A7 and A8 reveal the background uniformity variation corresponding to variations perceived at a large viewing distance. Detail signals, D1 to D8, represent the high frequency components at different resolutions. Their relative strengths can be seen in Figure 6. To characterize the severity of the non-uniformity, standard deviations (SD) were computed on each of the approximation signals and plotted in Figure 7. Generally, SD decreases as resolution decreases, i.e. as relatively high frequency components are removed.

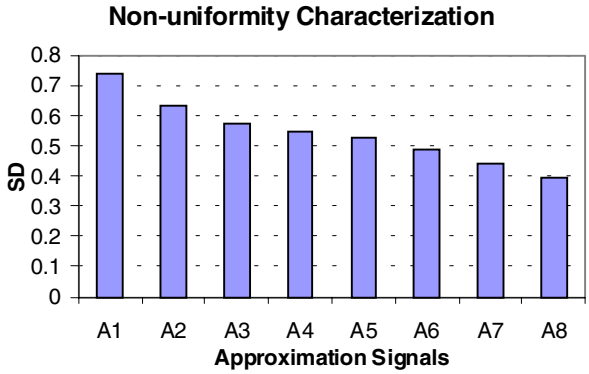

Figure 7. Non-uniformity characterization over a range of resolutions..

Similarly, as in previous studies,[2] the human visual transform function can be applied as a weighting factor. The data in Figure 7 corresponds to the non-uniformity perceived by a human observer at various viewing distances; e.g. the SD of signal A4 is the non-uniformity seen from a normal viewing distance, the SD of signal A3 is the non-uniformity seen at a close-up viewing distance, etc…

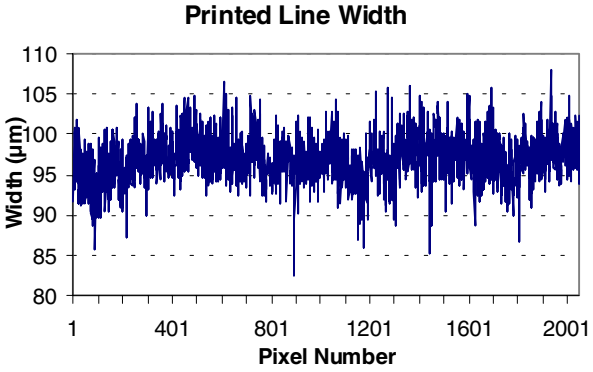

Figure 8. Line width measurements.

LED Printhead Evaluation using Line Width Measurement

The quality of an LED print head can be evaluated by activating individual LED elements selectively in a designed line pattern. The width of the produced lines correlates with LED intensity, while the position of the produced lines indicates LED position accuracy. Figure 8

shows the width of each line measured in this study. It shows that line width is not uniform and has high and low frequency variations. Similarly, the line width versus pixel number signal can be analyzed by wavelet decomposition as shown in Figure 9. Note that only the approximation signals are plotted. Mid-resolution variation is our major concern because they correspond to objectionable vertical banding. The standard deviations for these approximation signals are plotted in Figure 10. For quality control purposes, a threshold could be established at the appropriate resolution level which correspond to the most objectionable defects (e.g. A4). A SD on line width exceeding this threshold would be judged as unacceptable.

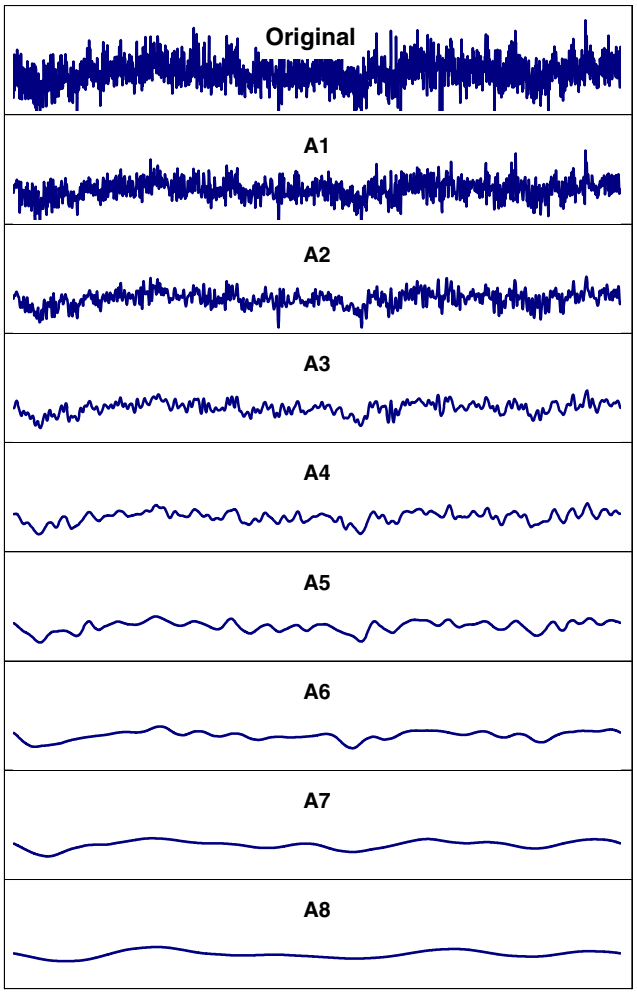

Figure 9. Wavelet decomposition of line width measurements.

Correlating Print Uniformity with Line Width Measurement

In order to investigate the impact of LED array quality on print uniformity, correlation analyses were performed using the reflectance profile and the line width signal at mid-resolution using low-pass filtering to eliminate the high-frequency components. After adjusting the registration of starting point, ending point and scaling, the results are illustrated in Figure 11.

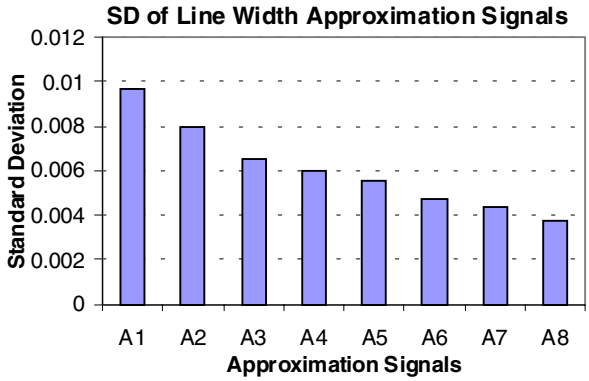

Figure 10. Line width uniformity characterization at various resolutions.

It can be seen that reflectance is inversely correlated to line width. LED pixels which produced relatively wide lines on the line target also cause dark bands on the 50% gray print. Figure 12 plots the line width versus measured reflectance. Although there is significant scatter present in the data, it still shows that there is a strong correlation between the line width measurements and the reflectance profile. This suggests that the primary cause of the non-uniformity on the 50% gray page at perceivable frequencies also causes non-uniform line widths. Since each of the lines in question is printed by a single pixel, it is most likely non-uniformity in the size or intensity of individual LED pixels which is primarily responsible for the non-uniformity in the 50% gray page. The slope of the correlation in Figure 12 indicates that a 10 μm change in line width corresponds to a 3% reflectance change (on a gray area with nominal reflectance of 10%). However, the relationship between printed line width and the width and intensity of the pixels on the LED print head is complicated by the presence of optics and the photosensitivity of the photoconductor.

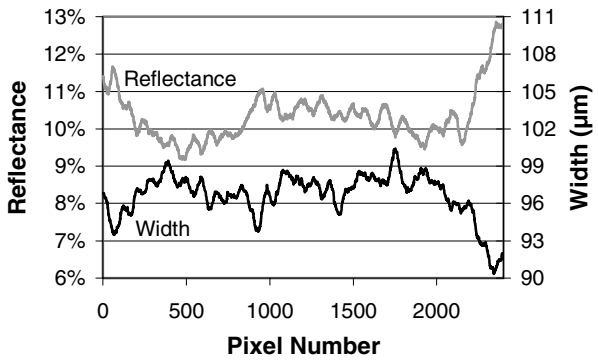

Figure 11. Line width measured on the line pattern test print and reflectance measured across the 50% gray test print. High frequency components have been removed by a low-pass filter (compare with Figs. 3 and 8).

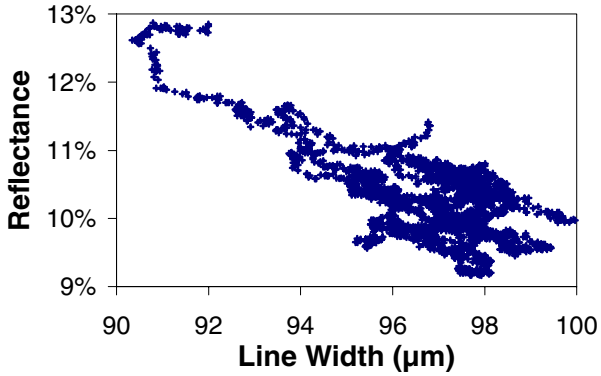

***Figure 12**. Reflectance measured across the 50% gray test print correlated with line width measured on the line pattern test print. High frequency components have been removed by a low-pass filter.*

Direct LED Pixel Measurement

Direct LED inspection verified our methodology of the indirect approach. Using direct inspection, the individual LED element positions were determined. The center to center spacing of 13 adjacent pixels is shown in Figure 13. The data plotted in Figure 13 correspond to a junction between two LED integrated circuits (ICs). Pixels with an index below 7 belong are located on the first IC chip and pixels with an index of 7 and higher are located on the second IC chip. The gap between the two adjacent ICs (pixel index 7) can clearly be seen in this chart. From the position data, the error of each individual pixel can also be estimated. These positional errors will produce non-uniformity in a solid print (e.g. the 50% gray print sample), but they are not necessarily revealed by measuring the width of lines printed by individual pixels. Therefore, the spacing errors like the one shown in Figure 13 are likely one of the secondary effects responsible for the scatter in Figure 12.

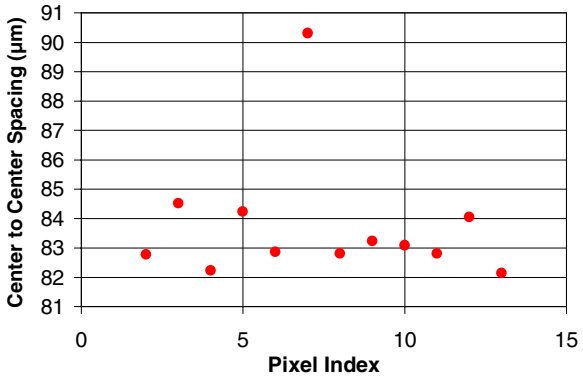

***Figure 13**. Pixel spacing measured directly on LED printhead.*

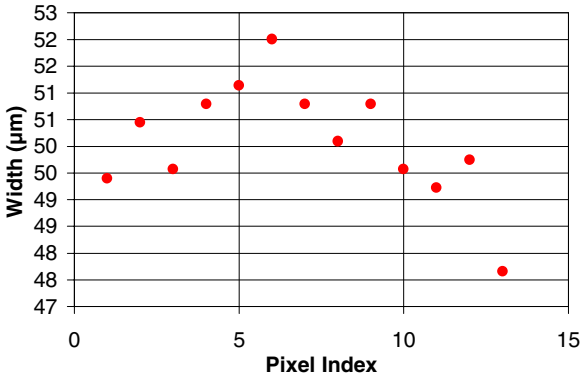

***Figure 14**. Pixel width measured directly on LED printhead.*

As mentioned previously, the detailed relationship between pixel size/intensity and printed line width is quite complicated, but the existence of such a relationship is without question. The width of individual pixels measured directly on the LED print head is shown in Figure 14. Note that the actual pixel size is approximately 50 µm, while the resulting printed lines are approximately 100 µm wide (see Figure 8). The data show approximately an 8% range in the variation of line width for this LED array.

Conclusions

In this paper we illustrated the techniques of LED printer and print head quality evaluation using print quality analysis. A well-designed test target combined with a powerful print quality measurement tool is the key for successful evaluation and root-cause diagnosis. Although only an LED printer was used in this investigation, the methodology can be applied to other types of printer as well. For ink-jet or thermal printers, banding caused by paper incrementing error or print head defects might be analyzed similarly. This paper also explored the application of wavelet transform for multi-resolution analysis. The results show that DWT provide an efficient tool in decomposition and data analysis.

References

1. David J. Forrest, John C. Briggs, Ming-Kai Tse, and Steve Barss "Print Quality Analysis as a QC Tool for Manufacturing Inkjet Print Heads", IS&T's 14, 1998 International Conference on Digital Printing Technologies, Toronto, Canada
2. John C. Briggs, Mike Murphy and Yichuan Pan, "Banding Characterization for Inkjet Printing", PICS 2000, Portland, Oregan
3. S. Mallat, "A Wavelet Tour of Signal Processing", Academic Press, 1998

Biography

Dr. Luo Cheng joined QEA in January 2001 as Director of R&D. Prior to coming to QEA, he worked at Lexmark International Inc. as a technical leader in the areas of image/print quality research, automated printing quality analysis system and intelligent diagnostic system development. Luo Cheng received his BS degree in textile engineering from China Textile University, MS and Ph.D in a combined program in textile science and electrical engineering from the University of Tennessee at Knoxville.